http://dx.doi.org/10.5516/NET.07.2012.009

NANO-STRUCTURAL AND NANO-CHEMICAL ANALYSIS OF NI-BASE ALLOY/LOW ALLOY STEEL DISSIMILAR METAL WELD INTERFACES

KYOUNG JOON CHOI, SANG HUN SHIN, JONG JIN KIM, JU ANG JUNG, and JI HYUN KIM*
Interdisciplinary School of Green Energy, Ulsan National Institute of Science and Technology (UNIST)
Ulju-gun, Ulsan Metropolitan City 689-798, Republic of Korea
*Corresponding author. E-mail : kimjh@unist.ac.kr

Received February 07, 2012
Accepted for Publication March 19, 2012

The dissimilar metal joints welded between Ni-based alloy, Alloy 690 and low alloy steel, A533 Gr. B with Alloy 152 filler metal were characterized by using optical microscope, scanning electron microscope, transmission electron microscope, secondary ion mass spectrometry and 3-dimensional atom probe tomography. It was found that in the weld root region, the weld was divided into several regions including unmixed zone in Ni-base alloy, fusion boundary, and heat-affected zone in the low alloy steel. The result of nanostructural and nanochemical analyses in this study showed the non-homogeneous distribution of elements with higher Fe but lower Mn, Ni and Cr in A533 Gr. B compared with Alloy 152, and the precipitation of carbides near the fusion boundary.

KEYWORDS : Dissimilar Metal Weld, Scanning Electron Microscope, Secondary Ion Mass Spectrometry, Transmission Electron Microscope, 3-Dimensional Atom Probe Tomography, A533 Gr. B, Alloy 152, Stress Corrosion Cracking

1. INTRODUCTION

Dissimilar Metal Welds (DMWs) is generally applied to nuclear power plants for manufacturing and machining in structural components such as reactor pressure vessel and Pressurizer nozzles. Alloy 152 is used frequently as filler metal in the manufacture of the DMW in light water reactor to join the low alloy steel pressure vessel nozzles and steam generator nozzles to nickel-based wrought alloy or austenitic stainless steel components. The thermal expansion coefficient of the alloy lies between ferrite steel and austenitic stainless steel. It also significantly retards carbon diffusion from the ferrite base metal to the weld metal [1, 2]. However, in recent years cracking phenomena have been observed in the welded joints. Concerns have been raised to the integrity and reliability in the joint transition zone due to the high susceptibility of the heat affected zone (HAZ) and the fusion boundary (FB) to stress corrosion cracking (SCC) in combination with thermal aging [1, 3-5].

The DMW has some characteristics in its microstructure and properties [1, 3, 6]. Firstly, there exists the composition gradient from the base metal to the weld metal across the FB. Such a change of the composition causes the change in the microstructure, mechanical property as well as the corrosion resistance. Secondly, the DMW is exposed to the thermal cycling during the welding [3, 7]. Thermal cycling during the weld process makes the change in the microstructure, mechanical properties and the corrosion resistance. Koo et al. [7] found that in a single-pass weld of structural steels four distinct zones of the HAZ are formed by the local thermal cycle experienced during welding. The four zones consist of coarse grain zone, fine grain zone, inter-critical zone, and sub-critical zone. The HAZ in low alloy steel showed higher level or density of hardness than the base metal. Thirdly, the formation of residual stress in the FB region due to the microstructure heterogeneity and the thermal mismatch can result in the gradient of mechanical properties across the FB [8].

Since the material microstructure and chemical composition are key parameters affecting the SCC, improving the understanding of SCC at the FB region requires fundamental understanding of the unique microstructure of the FB region in DMW. Hou et al. [1] found that scanning electron microscope (SEM), transmission electron microscope (TEM) and energy-dispersive X-ray spectroscopy (EDS) analysis showed the composition gradient and microstructure near the FB in a dissimilar weld joint of Alloy 182-A533 Gr. B. In the SEM and TEM analysis of the study, the unidentified band and the chromium carbides have been discovered near the FB in the low alloy steel HAZ. Although the SCC was usually confined to and initiated from the weld metals [9], the FB is also a potential path of cracking

[10]. Despite the potential degradation and consequent risk in the DMW, there is still a lack of the fundamental understanding of microstructure in the FB region, in particular, in the region containing unidentified band structure near the FB.

Therefore, the current study is aiming at the characterization of the dissimilar metal joints which were welded between Ni-based alloy, Alloy 690 and low alloy steel, A533 Gr. B with filler metal, Alloy 152 by using nanostructural and nanochemical analyses including optical microscope, SEM, TEM, secondary ion mass spectrometry (SIMS) and 3-dimensional atom probe tomography (3-D APT).

2. EXPERIMENT

2.1. Materials

A representative dissimilar weld mock-up made of Alloy 690/Alloy 152/A533 Gr. B was fabricated and provided by Argonne National Laboratory (ANL). A533 Gr. B was coated with Alloy 152 with the process of shielded metal arc welding followed post welding heat treatment by at 607~635ºC for 3 hours. After the process, the weld joint of Alloy 690 and A533 Gr. B was prepared by the shielded metal arc welding method with Alloy 152 fillers. The first weld layer was buttered with voltage of 25-26 V, current of 97-102 A, travel speed of 127mm/min, and maximum heat input of 1.252 KJ/mm. Then, the remainder was welded with the same range of voltage, maximum heat input and travel speed as initial buttering, but with current of 97-102 A and the maximum heat input of 1.437KJ/mm. During the process, the interpass temperature was kept below 199ºC, and the minimum of preheat temperature is 20ºC. Chemical compositions of both metals are shown in Table 1. The sample containing the interface and Alloy 152 was cut from the dissimilar weld joint as shown in Fig. 1.

Table 1. Chemical Composition (in wt. %) of Dissimilar Metal Weld used in this Study

Material	Composition													
	C	Al	Si	P	S	Cr	Mn	Fe	Co	Ni	Cu	Nb+Ta	Mo	Ti
Alloy 690	0.03		0.07		<0.001	29.5	0.20	9.9		59.5	0.01			
Alloy 152	0.040	0.240	0.460	<0.003	<0.001	29.040	3.560	9.360	<0.01	55.25	<0.01	1.84	0.01	0.15
A533 Gr. B	0.220		0.19	0.010	0.012	0.18	1.28			0.51			0.48	

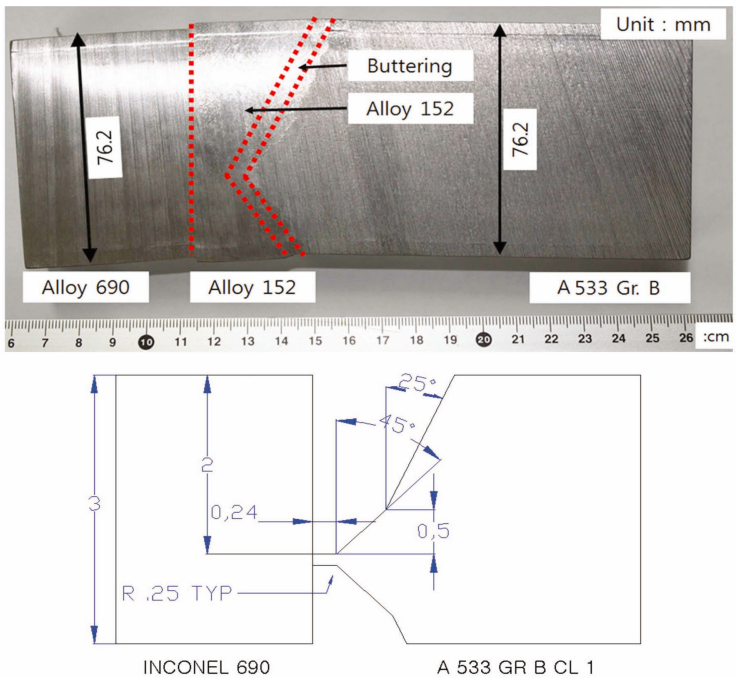

Fig. 1. Blue Print and Cross Section of Alloy 690-Alloy 152-A533 Gr. B Dissimilar Metal Weld (DMW)

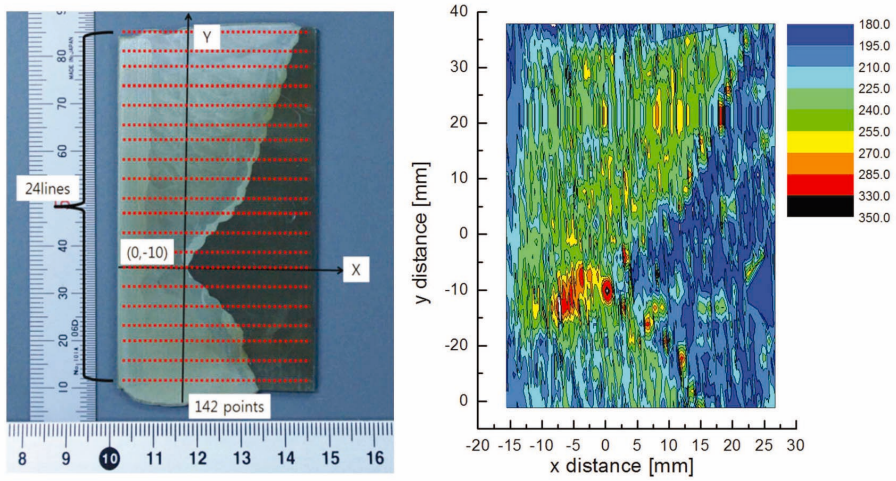

(a) (b)

Fig. 2. Microhardness Measurement Position (a) and Microhardness 2D Distribution (b) in the DMW

2.2 Specimens

The specimen for microhardness and SEM analyses was prepared by polishing the sample with ~0.05μm colloidal silica. The specimen for SEM was prepared by etching using a 3% nital solution. The specimen for SIMS was prepared by polishing the sample with ~0.05μm colloidal silica. The specimens for TEM and 3D APT were prepared by using focused ion beam for thinning. TEM specimens were deposited with carbon, cut and thinned with gallium ion beam by using Quanta 3D FEG focused ion beam. The specimens were about 100nm thick. 3D APT specimens were deposited with platinum, cut and thinned with gallium ion beam by Helios Nanolab 600 dual-beam focused ion beam. The specimens have a needle shape of about 100 nm in diameter.

2.3 Procedure

Vickers microhardness measurement was performed with 0.3 kgf(=2.94N) of test load during 10 sec per each position. The number of positions for measurement is 142 points per a horizontal line. There are 24 horizontal lines for the measurement as shown Fig. 2 (a). The distance between each horizontal line is 3 mm, and that between each point in each horizontal line is 0.3 mm. The procedure is followed by ISO-6507-1. Metallographic microstructure of the FB region was characterized by SEM. Chemical composition in the FB region was analyzed by (Quanta 200 SEM) EDS. The elemental map of alloy constituents was characterized by SIMS (CAMECA, IMS 6F SIMS) in positive as well as negative mode. While the positive mode uses O^+ gun, a voltage of 7.5kV and a current of 200pA (detected ion: 52Cr, 55Mn, 56Fe, 58Ni, 98Mo), the negative mode uses Cs+ gun, a voltage of 15kV and a current of 20pA (detected ion: 1H, 12C, 16O, 28Si). A

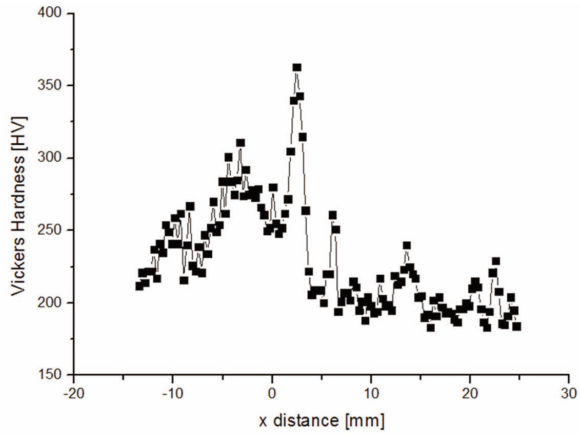

Fig. 3. Microhardness Profile across in the Weld Root Region in the DMW

JEM-2100F TEM was used for analyzing the transition of crystallographic microstructure and chemical composition in the FB region.

A LA_WATAP was used for the 3-D APT analysis of the chemical composition in the region containing the A533 Gr. B and the FB by utilizing laser pulsing with a wavelength of 343 nm. The analyses were made at a temperature of -213ºC, and the pulse frequency and the voltage range are 100 kHz and 2~14kV, respectively.

3. RESULT

3.1 Microhardness Measurement

Fig. 2 (b) shows the result of 2-dimensional distribution of measured Vickers microhardness values in the weld region, and Fig. 3 shows the linear profile of measured

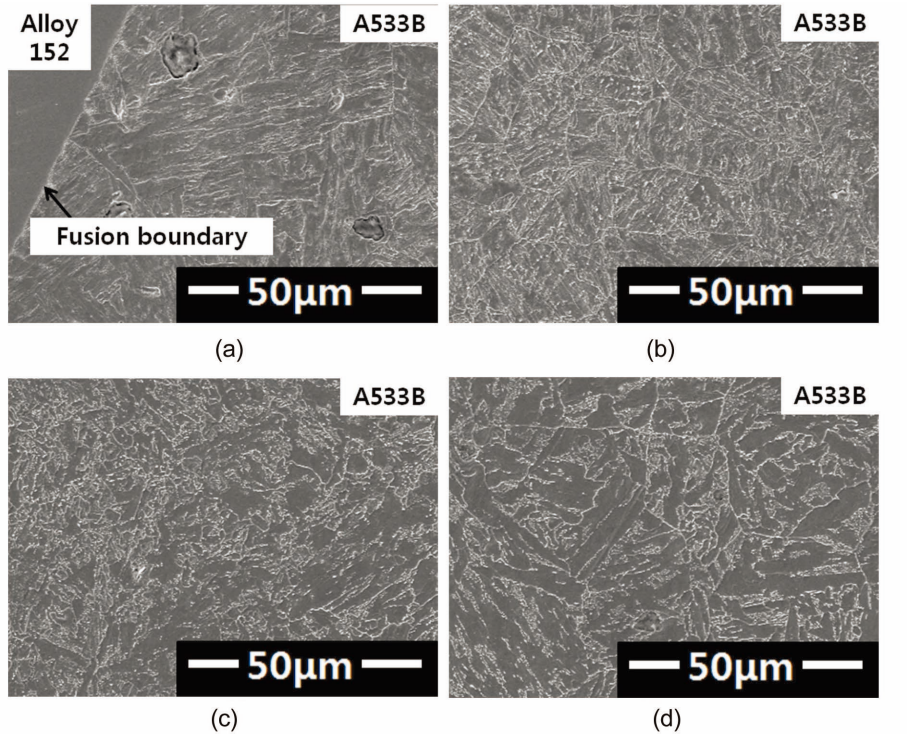

Fig. 4. SEM Images of the FB to A533 Gr. B Coarse Grained HAZ (a), Fine Grained HAZ (b) with about 200μm, Inter-critical HAZ (c) with about 400μm, Sub-critical HAZ (d) with about 600μm from the FB

microhardness in the weld root region. It is observed that the microhardness in the Alloy 152 weld is generally larger than that of the A533 Gr. B base metal. Also, there exist two narrow regions in the HAZ of A533 Gr. B which compared with other regions showing very higher peaks of hardness. The range of measured Vickers hardness in Alloy 152 weld region is between 200 and 300, and that of A533 Gr. B base metal is around 200 except the HAZ region near the FB. The first and largest peak in the HAZ in A533 Gr. B is around 370 in Vickers hardness, and the second peak is around 270 in Vickers hardness, which is about the same range as that in the weld region. Even though it would be difficult to directly correlate the hardness measurement to the nanosize precipitates distribution, the local peaking of hardness in the HAZ where is located very adjacent to the FB can give the insight for the general material properties with less ductility around the region. Moreover, the region in the HAZ showing the highest hardness value can be possibly degraded by thermal aging with the combination of weld thermal history. Previous studies [11, 12] have observed that the heat affected zone is experiencing of thermal aging which can induce the grain coarsening, the precipitation and the segregation of trace impurities. Local loss of ductility judged from measured higher hardness is considered to be more problematic in terms of structural integrity, synergistically combined with the effect of thermal aging near the FB. Therefore, it is considered that thermal aging can cause the degradation in the higher hardness region. Therefore, the current study including detail microstructure analysis is primarily focused on this region.

3.2 Microstructural Analysis by SEM

Fig. 4 represents SEM images showing four distinguished regions between the FB and the HAZ in A533 Gr. B; coarse grained HAZ, fine grained HAZ, inter-critical HAZ and sub-critical HAZ. Larger lath martensite structure is changed into bainite (base metal) consisting of ferrite and cementite. Comparing the profile of microhardness measurement shown in the previous section, the peak of microhardenss is corresponded to the coarse grained HAZ having larger lath martensite structure , and the relatively low microhardness region is to banite structure in the HAZ. Fig. 5 shows the typical SEM microstructural images around the weld root region near the FB. The microstructure contains ferrite structure having 10~15μm size. In the structure near the FB, the peak of microhardness was similary observed as shown in the previous section.

Figs. 6 and 7 show the EDS elemental analysis across the weld, showing that Fe content is higher, but Cr, Ni and Mn contents are lower in A533 Gr. B than in Alloy 152 as expected. However, an ‘unmixed zone’ showing a feature of island, which possesses similar chemical composition with A533 Gr. B as shown in Fig. 7, is also observed.

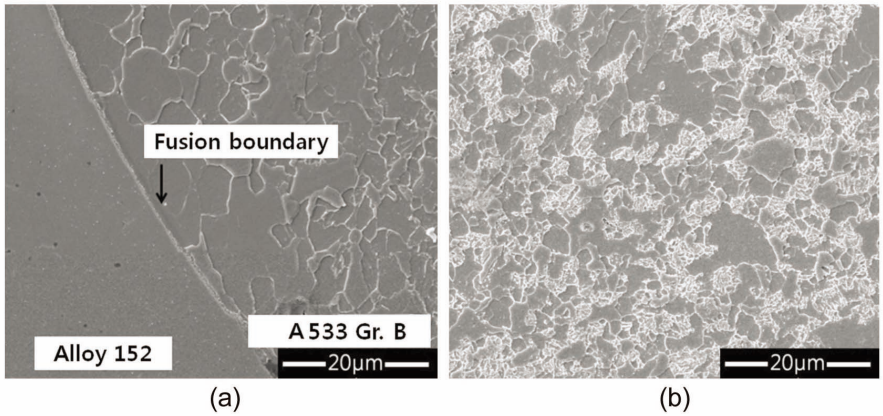

Fig. 5. SEM Images of near the FB (a), 80 μm from the FB (b) to A533 Gr. B in the Weld Root

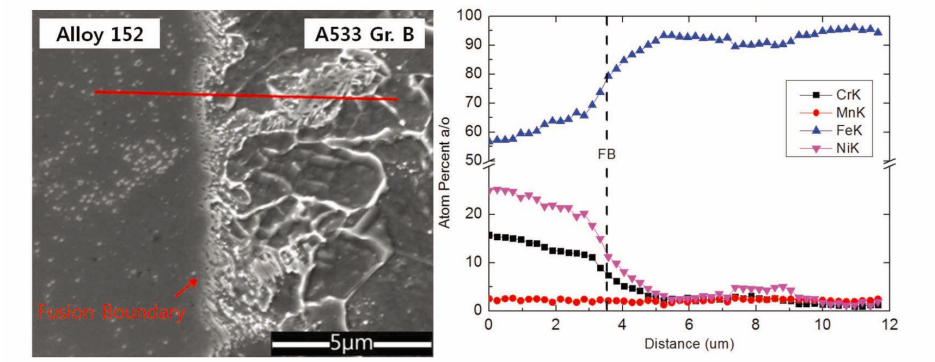

Fig. 6. SEM EDS Analysis Result across Weld Root (Smooth Transition of EDS Profiles)

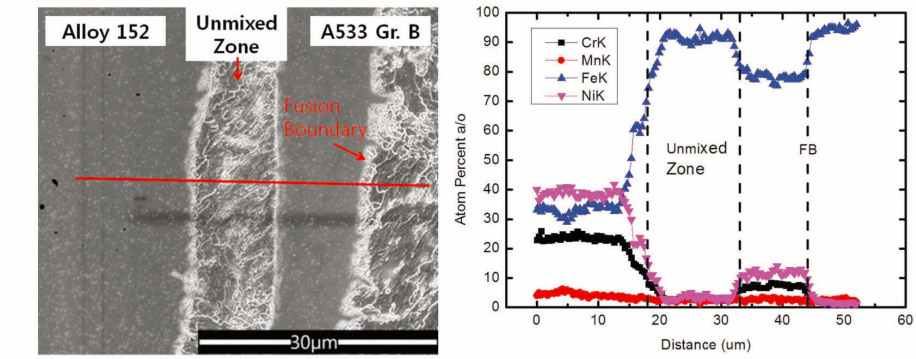

Fig. 7. SEM EDS Analysis Result across Weld Root (Unmixed Zone)

3.3 Microstructural Analysis by SIMS

Two different modes were used for SIMS analysis in this study. For heavy elements, the positive mode was used and the results are shown in Fig. 8. Similarly during the SEM analysis, a higher Fe content was observed, while Cr, Ni and Mn contents are lower in A533 Gr. B than in Alloy 152. For the light element, the negative mode was used and the results are shown in Fig. 9. From Fig. 9, carbon is accumulated in weld very close to the FB than other regions. In the previous study by Hou et al. [1], they reported the chromium carbides on the FB between Alloy 182 filler metal and A533 Gr. B, as similar to the observation in this study. It is believed that the higher concentration of carbon in the side of A533 Gr. B is caused during the

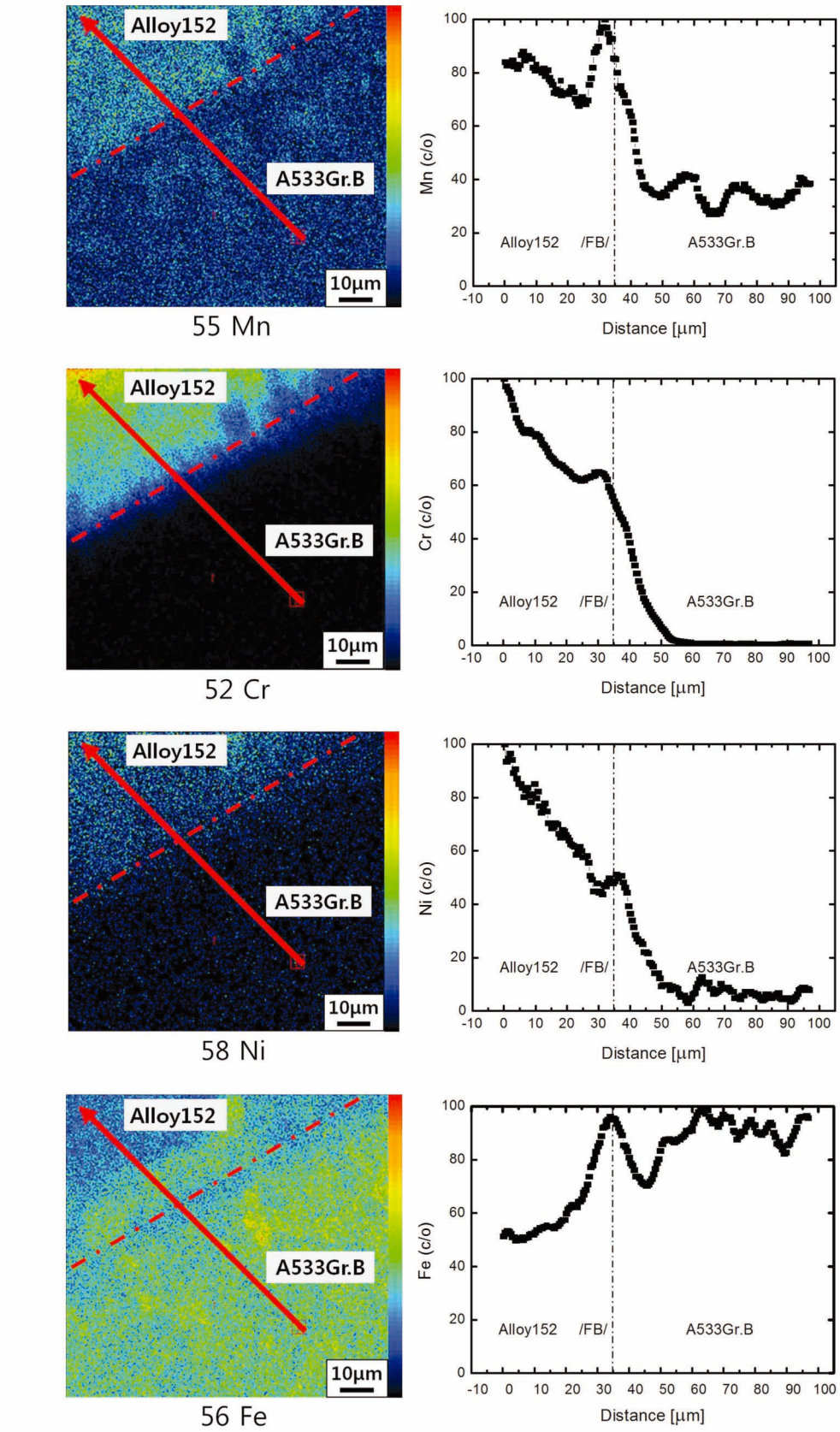

Fig. 8. SIMS Images for Cr, Mn, Fe and Ni Distributions across Weld Root in Positive Mode (100μm × 100μm)

welding process by the formation of carbide through the reaction between carbon and alloying elements (Cr, Mo, and Mn) in Alloy 152 weld metal.

3.4 Microstructural Analysis by TEM

The result of TEM-EDS analysis shows the consistency to that of SEM-EDS and SIMS analysis in this study. As shown in Fig. 10, it is found that there exist sharp transitions of chemistry depending on positions and elemental species near the FB in the DMW. It is also observed that there exist regions showing a valley of Fe and a peak of C, Cr, Mn and Mo in the alloy constituent distribution. The transitional region is considered to correspond to carbide precipitates near the FB in the weld. As shown in Fig. 10, the several precipitates on the fusion boundary were observed. The low precipitate density on fusion boundary is most

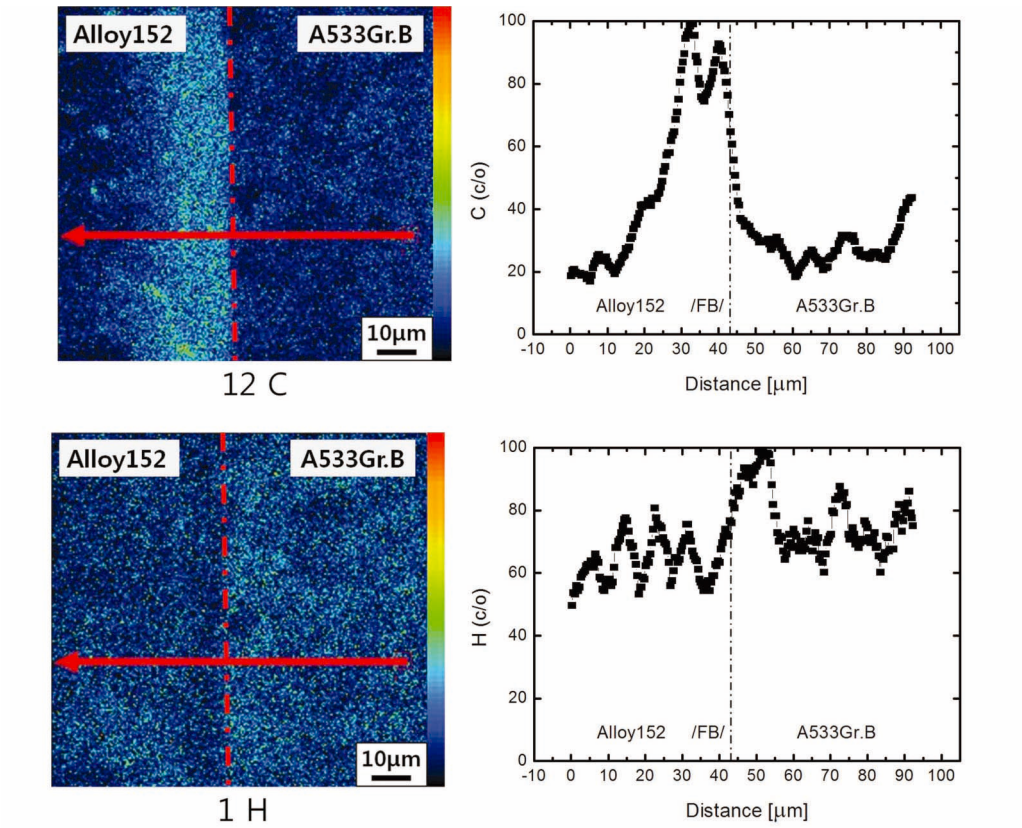

Fig. 9. SIMS Images for H and C Distributions across Weld Root in Negative Mode (100μm × 100μm)

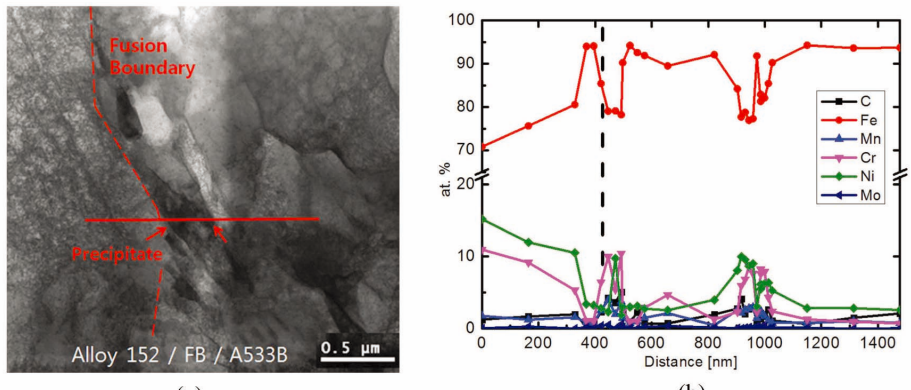

(a) (b)

Fig. 10. TEM Micrograph in Dark field (a), and Elemental Distributions by EDS (b) in the Fusion Boundary of DMW

likely due to the high solubility of carbon in the side of low alloy steel having bcc structure. In addition, the TEM observation also shows that the structure is mainly B.C.C. with lath martensites in the low alloy steel side.

3.5 Microstructural Analysis by 3-D APT

Fig. 11 shows the 3-dimensional distribution of atomic species around the weld fusion boundary measured by 3D APT. Fig. 11 (a) displays the three dimensional reconstruction of the DMW specimens and interesting regions for the further detail analysis as summarized in Table 2. Fig. 11 (b) presents each elemental distributional map including C, Cr, Mn, Mo, Si, Fe and Ti. Table 2 includes the atomic concentrations of the each region. Figs. 11 (c) and (d) the elemental profiles in the volumes of 'F-E' and 'C-D-E' represented in Fig. 11 (a). As can be seen from Figs. 11 (c) and (d), it is observed that the carbon and chromium concentrations are higher near the FB than near other regions, which is similar to what's observed in SIMS negative analysis. Table 2 shows that the higher concentrations of Cr, C, Mo and Mn are in the spaces of A, C, E and G. As seen from the 3D APT results, these regions can be considered as carbide precipitates which are formed in Alloy 152 weld metal during the welding process. In addition, through that B and D spaces have higher Fe and lower Ni than F space in Figs 11 (c) and (d) and Table 2, the FB can be also distinguished from other regions as shown in Fig. 11 (a). There are a detail procedure for the 3-D APT analysis including sample preparation and analysis condition, and the results will be published in the separate article in the future.

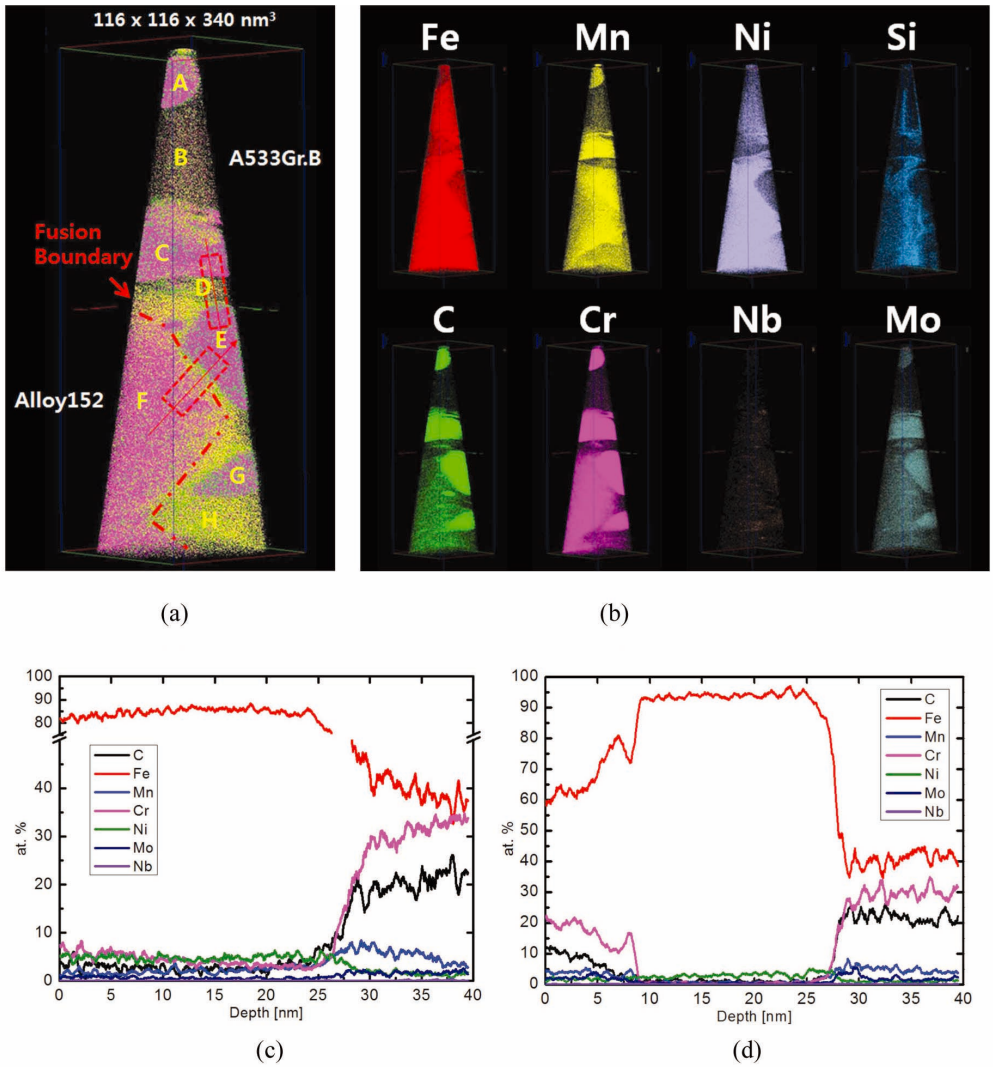

Fig. 11. 3-D Reconstruction of the DMW Atom Probe Specimen (a), the Elemental Distributional Map of Fe, Mn, Cr, C, Mo, Ni, Si and Nb Distributions (b), and Elemental Profiles in the Volume of 'F-E' (c) and 'C-D-E' (d)

4. DISCUSSION

This study is focused on the nanostructural & nanochemical analysis near the FB between Alloy 152 and A533 Gr. B to evaluate the integrity of the Alloy 152-low alloy steel DMW. By the clear understanding of the microstructure of the fusion boundary region in an Alloy 152-low alloy steel dissimilar weld joint, the results are discussed in this section under the context of the likely effect of long term aging on the potential degradation and cracking in HAZ. From the results described in the previous section, it can be summarized that there exists the region showing the highest microhardness, and chromium carbides were observed in the FB as well as in the HAZ where is located very close to FB.

In previous studies by Nelson et al. [10], they investigated the FB in ferritic-austenitic DMW by using 70Ni-30Cu filler metal and iron base metal. Their findings showed that the FB exhibited random misorientation between the base and the weld metal grain. They concluded that the type-II boundary that parallels to the fusion boundary in the dilution zone (DZ) of weld metal could play a role of a potential crack path and had been formed as a result of the occurrence of the allotropic transformation at elevated temperatures. Hou et al. [1] performed similar experimental study with Alloy 182 filler metal and A533 Gr. B. They also found the existence of a type-II boundary parallel to the FB in the dilution zone of Alloy 182. They observed the precipitates of composited carbides of Ti and Nb, and $Cr_{23}C_6$ on the type-II boundary and FB region. Near the type-II boundary and FB region, the formation of precipitates can cause the depletion of chromium in the matrix, which may result in the less formation of protective chromium oxide layer in the high temperature aqueous environment. The region in the HAZ showing the highest hardness may have degraded through thermal cycling during the weld process with the combination of high residual stress. The long term exposure of this king of material could experience the thermal aging which can form the chromium carbides near the FB by promoting the diffusion of C content at the service temperature [13, 14]. Additionally, in regards to the crack parallel to the FB, Seifert et al. [13, 14] evaluated the cracking behavior in the transition region of an Alloy 182/ SA 508 cl.2 DMW. The growth rate of SCC in a high-purity water environment was only slightly higher parallel to FB than in the dilution zone. Combining all described above, the FB in the DMW can be severely degraded by the decreased resistance to intergranular stress corrosion cracking. However, a detail investigation on the effect of thermal aging on the change of properties in the DMW needs to be pursued to warrant the integrity of DMWs.

5. CONCLUSION

Nanostructural and nanochemical analysis were performed to characterize the fusion boundary of as-welded dissimilar metal weld which consists of Ni-base alloy and low alloy steel. The techniques used in this study include the microhardness measurement, scanning electron microscopy (SEM), secondary ion mass spectroscopy (SIMS), transmission electron microscopy (TEM), and 3-dimensional atom probe tomography (3-D APT). The conducted microhardness measurements in the region of heat affected zone (HAZ) of A533 Gr. B revealed the existence of the highest Vickers microhardness region in the HAZ. By SEM and SIMS analyses, Fe content was found to be higher than Alloy 152. But Cr, Ni and Mn contents probed to be lower in A533 Gr. B than in Alloy 152 as the chemical composition of the metals. From TEM and 3-D APT analyzed, the chromium carbides on the fusion boundary were observed. The long term exposure of this kind of DMW could experience the thermal aging

Table 2. 3D APT Elemental Concentration (in at. %) in the Each Region Indicated in Fig. 11

Position	Element									
	Cr	Mn	Fe	Ni	Mo	C	Nb	Si	O	Al
A	31.697	4.674	37.958	1.483	1.275	22.399	0.042	0.311	0.129	0.033
B	0.414	0.697	95.919	1.949	0.147	0.543	0.015	0.204	0.112	0
C	29.086	6.059	41.499	1.044	2.308	19.606	0.053	0.200	0.121	0.025
D	0.361	0.621	93.754	2.975	0.382	0.945	0.052	0.858	0.041	0.011
E	31.717	4.621	38.210	1.112	2.118	21.801	0.080	0.208	0.086	0.028
F	4.428	1.740	84.657	5.224	0.552	2.740	0.034	0.553	0.071	0.002
G	16.674	2.179	58.207	1.839	2.459	18.07	0.292	0.174	0.071	0.035
H	0.582	0.679	92.211	3.380	0.268	1.914	0.037	0.869	0.061	0

which can cause the degradation by grain coarsening, the precipitation and the segregation of trace impurity near the FB. Also, the local loss of ductility judged from measured higher hardness is considered to be more problematic in terms of structural integrity, synergistically combined with the effect of thermal aging near the FB, even in case of no local depletion of chromium. However, a detail investigation on the effect of thermal aging on the change of properties in the DMW needs to be pursued to warrant the integrity of DMWs

ACKNOWLEDGEMENT

This work was financially supported by the R&D Program of Korea Institute of Energy Technology Evaluation and Planning (KETEP) funded by the Ministry of Knowledge Economy (MKE) and by the Korean Nuclear R&D program organized by the National Research Foundation (NRF) of Korea in support of the Ministry of Education, Science and Technology (MEST).

REFERENCES

[1] J. Hou, Q.J. Peng, Y. Takeda, J. Kuniya, T. Shoji, J.Q. Wang, E.H. Han and W. Ke, "Microstructure and mechanical property of the fusion boundary region in an Alloy 182-low alloy steel dissimilar weld joint," J. Mater. Sci., vol. 45, pp. 5332 (2010)

[2] M. Sireesha, S.K. Albert, V. Shankar andS. Sundaresan, "A comparative evaluation of welding consumables for dissimilar welds between 316LN austenitic stainless steel and Alloy 800," J. Nucl. Mater., vol. 279, pp. 65 (2000)

[3] J.W. Kim, K.S. Lee, J.S. Kim and T.S. Byun, "Local mechanical properties of Alloy 82/182 dissimilar weld joint between SA508 Gr.1a and F316 SS at RT and 320 ^{o}C," J. Nucl. Mater., vol. 384, pp. 212 (2009)

[4] J.I. Bennetch, G.E. Modzelewski, L.L. Spain and G.V. Rao, "Root Cause Evaluation and Repair of Alloy 82/182 J–Groove Weld Cracking of Reactor Vessel Head Penetrations at North Anna Unit 2," ASME PVP, vol. 437, pp. 179 (2002)

[5] G.F. Li, J. Congleton, "Stress corrosion cracking of a low alloy steel to stainless steel transition weld in PWR primary waters at 2928C," Corrosion Sci., vol. 42, pp. 1005 (2000)

[6] C.H. Jang, J.H. Lee, J.S. Kim and T.E. Jin, "Mechanical Properties Evaluation in Inconel 82/182 Dissimilar Metal Welds," J. PVP, vol. 85, pp. 635 (2008)

[7] J.Y. Koo and A. Ozekcin, Welding Metallurgy of Structure Steels, p. 119, The Metallurgical Society, New Jersey (1987)

[8] H.T. Lee, S.L. Jeng, C.H. Yen and T.Y. Kuo, "Dissimilar welding of nickel-based Alloy 690 to SUS 304L with Ti addition," J. Nucl. Mater., vol. 335, pp. 59 (2004)

[9] H.P. Seifert, S. Ritter, T. shoji, Q.J. Peng, Y. Takeda and Z.P. Lu, "Environmentally-assisted cracking behaviour in the transition region of an Alloy182/SA 508 Cl.2 dissimilar metal weld joint in simulated boiling water reactor normal water chemistry environment," J. Nucl. Mater., vol. 378, pp. 197 (2008)

[10] T.W. Nelson, J.C. Lippold and M.J. Mills, "Nature and Evolution of the Fusion Boundary in Ferritic-Austenitic Dissimilar Metal Welds–Part 2: On-Cooling Transformations," J. Weld, vol. 79, pp. 267 (2000)

[11] J.H. Kim, Y.J. Oh and I.S. Hwang, "Fracture behavior of heat-affected zone in low alloy steels", J. Nucl. Mater., vol. 299, pp. 132 (2001)

[12] J.H. Kim and E.P. Yoon, "Notch position in the HAZ specimen of reactor pressure vessel steel", J. Nucl. Mater., vol. 257, pp. 303 (1998)

[13] J.D. Parker and G.C. Stratford, "Characterization of microstructures in nickel based transition joints," J. Mater. Sci., vol. 35, pp. 4099 (2000)

[14] J.D. Dupont and R. E. Mizia, "Review of Dissimilar Metal Welding for the NGNP Helical-Coil Steam Generator," INL/EXT-10-18459, Idaho National Laboratory (2010)